Inorganic Chemistry

Article

pubs.acs.org/IC

Effect of Substituents on the Water Oxidation Activity of $[Ru^{II}(terpy)(phen)Cl]^+$ Procatalysts

Dakshika C. Wanniarachchi, Mary Jane Heeg, and Cláudio N. Verani*

Department of Chemistry, Wayne State University, Detroit, Michigan 48202, United States

Supporting Information

ABSTRACT: A series of $[Ru^{II}(terpy\text{-}R)(phen\text{-}X)Cl]PF_6$ complexes was designed where terpy-R is the tridentate 4′-(4-methylmercaptophenyl)-2,2′:6′2″-terpyridine ligand MeMPTP and phen-X is a substituted phenanthroline with hydro (**1**), 5-nitro (**2**), 5,6-dimethyl (**3**), and 3,4,7,8-tetramethyl (**4**). This series allows us to compare the reactivity of phenanthroline-containing procatalysts with that of its well-established bipyridine counterparts as well as to study the effects of electron-withdrawing and -donating substituents on water oxidation. These species were thoroughly characterized by spectroscopic and spectrometric methods, and the structures of **1**, **3**, and **4** were determined by single-crystal X-ray diffraction. The procatalysts **1**−**4** show opposite trends compared to known terpyridine/bipyridine species; the unsubstituted procatalyst **1** yields a turnover number (TON) of 410 followed by 250 and 150 for complexes **3** and **4** with electron-donating substituents. Species **2**, with electron-withdrawing properties, yields the lowest TON of 60. Although the TONs decrease upon substitution, the presence of electron-donating methyl substituents enhances the rate of O_2 evolution during an early stage of catalysis. Interestingly, no evidence of conversion from chlorido-containing procatalysts into expected aqua-containing catalysts was observed for **1**−**4** by NMR and UV−visible spectroscopy during the induction period. This observation, along with reactivity toward $(NH_4)_2[Ce^{IV}(NO_3)_6]$, suggests that water nucleophilic attack happens to a high-valent ruthenium species rather than while at the Ru^{II} oxidation state. Reactivity follows a trend similar to the rate of O_2 evolution in all complexes. Furthermore, the electrospray ionization mass spectrometry and ^1H NMR analyses of **1**, as recovered after catalysis, indicate the presence of a chlorido ligand.

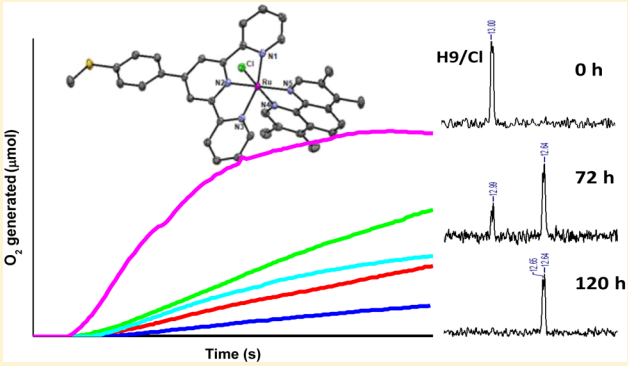

INTRODUCTION

Ruthenium-based catalysts have been avidly pursued in order to circumvent the steep thermodynamic requirements involved in water oxidation.[1] One of the most promising mononuclear topologies for such catalysts takes advantage of coordination of the bivalent ruthenium ion in an octahedral environment to polypyridine ligands such as terpyridine (terpy) and bipyridine (bipy) along with a monodentate aqua ligand occupying the sixth position. Therefore, $Ru^{II}(terpy)(bipy)X]^+$ procatalysts have been synthesized in which halogeno ligands X such as Cl, Br, and I occupy the sixth position.[2−4] In the presence of a sacrificial oxidant such as Ce^{IV} ions, these $[Ru^{II}(terpy)(bipy)\text{-}X]^+$ procatalysts require an induction period in which H_2O is believed to be incorporated, either by direct substitution of the halogen or by formation of a seven-coordinated intermediate.[2−4] Recent evidence suggests that direct substitution is favored by chorido-containing procatalysts, while seven coordination might be favored when heavier halogens such as iodides are present.[2−4] An alternative and less explored possibility is that partial displacement of flexible polypyridine ligands takes place. After water is coordinated, accepted mechanisms assume that proton-coupled electron transfer (PCET) leads to the formation of a $[Ru^{III}OH]^{2+}$ intermediate that is further oxidized to $[Ru^{IV}{=}O]^{2+}$ and $[Ru^{V}{=}O]^{3+}$. In the presence of water, the electrophilic pentavalent ruthenium oxo species can then be converted into hydroperoxo species $[Ru^{III}OOH]^{2+}$, which antecedes the formation of $[Ru^{IV}OO]^{2+}$ via another PCET step. At this point, O_2 can evolve via replacement by a water molecule, and the catalyst is then regenerated.[5−9] Optimization of the catalyst activity requires a balance between the availability of electron density at the metal center and limited π-back-bonding to the most labile ligand.[10] A certain balance can be achieved by the careful insertion of electron-donating and -withdrawing groups to each of the polypyridyl ligands. Similar groups can foster or prevent catalyst stability, depending on their position on either the bipy or terpy moiety, as seen in recent reports.[10,11] According to these findings, the insertion of electron-donating groups to terpy and electron-withdrawing groups to bipy should lead to a situation where the catalyst activity and stability are optimized. In this regard, we are interested in the electronic effects associated

Received: August 22, 2013
Published: March 19, 2014

   dx.doi.org/10.1021/ic402118u | *Inorg. Chem.* 2014, 53, 3311−3319

with the more rigid phenanthroline (phen) in $[Ru^{II}(terpy)(phen)Cl]^+$ procatalysts, both to evaluate their reactivity and because proper phen functionalization allows for the synthesis of multimetallic topologies.[12−16] While working on the functionalization of mercaptoterpyridines for self-assembly on gold electrodes, we noticed that the complex $[Ru^{II}(MeMPTP)(phen)Cl]PF_6$ [MeMPTP = 4′-(4-methylmercaptophenyl)-2,2′:6′2″-terpyridine)] showed catalytic activity toward water oxidation. We realized that this is a unique platform to (i) compare the effects of substituted phen with electron-donating and -withdrawing groups on the catalytic activities of the series of procatalysts summarized in Scheme 1, (ii) discuss the reactivity of these complexes toward Ce^{IV}, and (iii) evaluate the composition of the catalyst recovered after catalysis. The results follow.

Scheme 1. $[Ru^{II}(MeMPTP)(R\text{-}phen)Cl]PF_6$ Complexes with Substituted phen

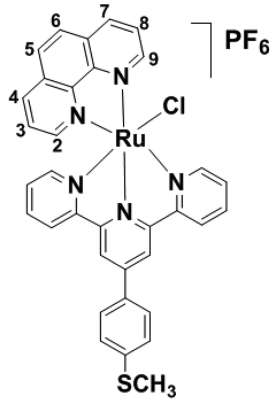

$[Ru^{II}(MeMPTP)(Phen)Cl]PF_6$ (1) -H
$[Ru^{II}(MeMPTP)(NO_2\text{-}Phen)Cl]PF_6$ (2) 5-NO_2
$[Ru^{II}(MeMPTP)(Me_2\text{-}Phen)Cl]PF_6$ (3) 5,6-Me
$[Ru(MeMPTP)(Me_4\text{-}Phen)Cl]PF_6$ (4) 3,4,7,8-Me

RESULTS AND DISCUSSION

Synthesis and Characterization of Ligands and Complexes. The ligand MeMPTP was synthesized as previously reported[17] and treated with 1 equiv of $[Ru^{II}(DMSO)_4Cl_2]$ (DMSO = dimethyl sulfoxide) to yield the precursor $[Ru^{II}(MeMPTP)(DMSO)Cl_2]$. Four complexes were obtained by reaction of the precursor with the appropriate phen ligand and further column-chromatographed to yield the high-purity species $[Ru^{II}(MeMPTP)(phen)Cl]PF_6$ (**1**), $[Ru^{II}(MeMPTP)(NO_2\text{-}phen)Cl]PF_6$ (**2**), $[Ru^{II}(MeMPTP)(Me_2\text{-}phen)Cl]PF_6$ (**3**), and $[Ru^{II}(MeMPTP)(Me_4\text{-}phen)Cl]PF_6$ (**4**). Species **1**−**4** were characterized by ^1H NMR and IR spectroscopies, high-resolution electrospray ionization mass spectrometry (ESI-MS), and elemental analysis prior to use, with excellent agreement between the different methods. Species **1**, **3**, and **4** were also characterized by X-ray crystallography.

Structural Characterization. X-ray-quality crystals of **1**, **3**, and **4** were obtained by the slow evaporation of a complex dissolved in acetonitrile (ACN) under dark conditions, as shown in Figure 1. The partial solution obtained for **1** does not allow for discussion of the bond lengths and angles, but it suffices to indicate connectivity, confirming the identity of the $[Ru^{II}(MeMPTP)(phen)Cl]^+$ cation (Figure S1 in the Supporting Information, SI). Complexes **3** and **4** show pseudooctahedral geometries around the ruthenium center, where the N_{terpy}−Ru bonds vary from 2.087(7) to 1.943(7) Å and relatively shorter bond lengths are observed for the central N atom of the terpy. Bond lengths for N_{phen}−Ru vary from 2.039(2) to 2.075(2) Å, where shorter bond lengths are observed for the N atom trans to the chlorido coligand. The difference in the bond lengths for the phen $N_{pyridine}$ located trans to Cl^- of **3** is 0.012 Å longer than that for **4**. These bond lengths are in good agreement with values reported in the literature.[18] The Ru−Cl bond length in complex **4** is shorter than that of **3** by ca. 0.05 Å. The molecular structures of **1**, **3**, and **4** clearly illustrate that the chlorido group is trans to the N4 atom of the phen.

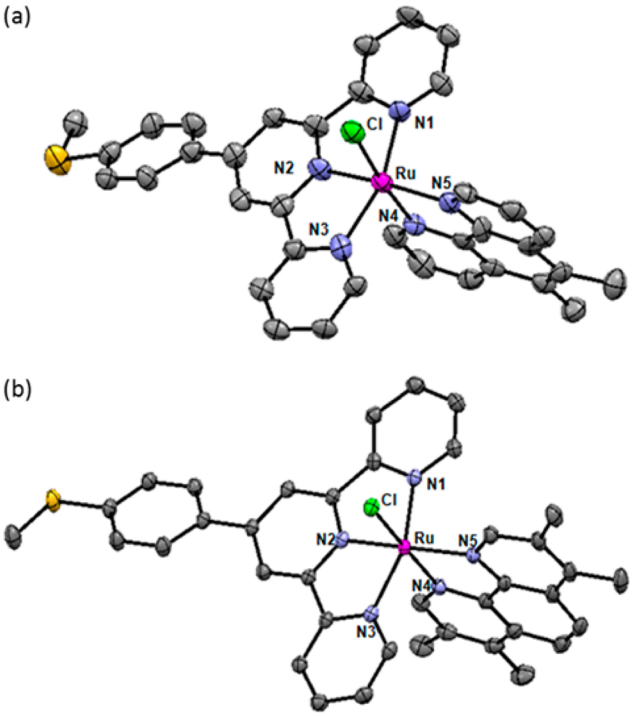

Figure 1. Molecular structure of the cations (a) $[Ru^{II}(MeMPTP)(Me_2\text{-}phen)Cl]^+$ ($\mathbf{3}^+$) and (b) $[Ru^{II}(MeMPTP)(Me_4\text{-}phen)Cl]^+$ ($\mathbf{4}^+$). Selected bond lengths (Å) and angles (deg): for $\mathbf{3}^+$, Ru−N1 = 2.087(7), Ru−N2 = 1.955(7), Ru−N3 = 2.058(8), Ru−N4 = 2.051(7), Ru−N5 = 2.072(7), Ru−Cl = 2.450(2) and N1−Ru−N2 = 79.1(3), N2−Ru−N3 = 79.9(3), N3−Ru−N5 = 98.5(3), N5−Ru−N1 = 102.4(3), N4−Ru−Cl = 173.8(2); for $\mathbf{4}^+$, Ru−N1 = 2.061(2), Ru−N2 = 1.943(2), Ru−N3 = 2.056(2), Ru−N4 = 2.039(2), Ru−N5 = 2.075(2), Ru−Cl = 2.407(7) and N1−Ru−N2 = 79.58(9), N2−Ru−N3 = 79.74(9), N3−Ru−N5 = 101.96(9), N5−Ru−N1 = 98.62(9), N4−Ru−Cl = 171.08(6).

Electronic and Redox Behavior. The efficiency of water oxidation in complexes **1**−**4** is sensitive to the electron density around the ruthenium center,[2,10,11] and the effect of electron-donating and -withdrawing substituents is reflected in the potential of the Ru^{II}/Ru^{III} couple, as measured in ACN and shown in Figure S2 in the SI. Complexes **1**−**4** display the Ru^{II}/Ru^{III} couple between 0.31 and 0.46 $V_{Fc^+/Fc}$. Another irreversible process consistently observed between 1.0 and 1.1 $V_{Fc^+/Fc}$ is attributed to oxidation of the $-SCH_3$ group of MeMPTP. The terpy/terpyridinium couple is observed around −1.94 to −2.14 $V_{Fc^+/Fc}$ for complexes **1**, **3**, and **4**. This process is absent for species **2**, which instead shows a process at −1.08 $V_{Fc^+/Fc}$ centered on the NO_2-phen ligand. In Figure 2, details are shown for the Ru^{II}/Ru^{III} couple, evidencing that the electron-withdrawing nitro group in complex **2** does not favor the

dx.doi.org/10.1021/ic402118u | Inorg. Chem. 2014, 53, 3311−3319

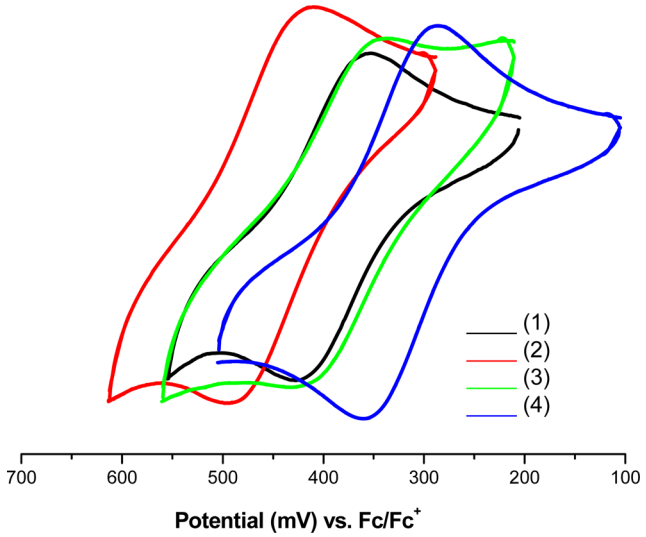

Figure 2. Cyclic voltammograms of the Ru^{II}/Ru^{III} couple for **1**−**4** in ACN/$TBAPF_6$ at 100 mV s^{-1}.

generation of a trivalent Ru^{III} state, as observed by the highest oxidation potential of 0.46 $V_{Fc^+/Fc}$. The unsubstituted **1** displays this couple at 0.40 $V_{Fc^+/Fc}$. An opposite trend is observed in the presence of weakly electron-donating methyl substituents in complexes **3** and **4**, yielding more affordable potentials of 0.38 and 0.33 $V_{Fc^+/Fc}$, respectively. The results in dichloromethane are shown in Figure S3 in the SI and show consistency with the above-mentioned behavior.

The UV−visible absorption spectra of complexes **1**−**4** were recorded in ACN and are shown in Figure S4 in the SI. The complexes show a pronounced band at 515−520 nm (Δ = 5 nm) due to ruthenium-to-terpy metal-to-ligand charge transfer (MLCT).[2,18,19] A second band is observed between 422 and 435 nm (Δ = 13 nm) and attributed to a MLCT process involving the ruthenium center and the phen ligand. This band has not been detected for **2** and is blue-shifted in **4** because of the presence of four electron-donating methyl groups. The fact that the second MLCT presents larger variance associated with the nature of the substituents on the phen ligand confirms that MLCT is associated with the Ru^{II} ← phen process.

Catalytic Activity toward Water Oxidation. The influence of electron-donating and -withdrawing groups in the catalytic properties of $[Ru^{II}(MeMPTP)(R\text{-}phen)Cl]PF_6$ complexes was evaluated by measurement of the turnover number (TON) = [generated O_2]/[catalyst] in moles) and of the rate of O_2 generation in solution. The TONs of these complexes were measured in 10 mL septum-capped round-bottomed flasks using $(NH_4)_2[Ce^{IV}(NO_3)_6]$ (550 mg, 1.0 mmol) and triflic acid (CF_3SO_3H, 3.0 mL, pH = 1) stirred together. An ACN solution of the complex under study (100 μL, 8×10^{-5} mmol) was added, and experiments were carried out under atmospheric conditions. The resulting mixture reacted 24 h, and then a sample of the headspace gas was collected and injected (100 μL) into a gas chromatograph. Atmospheric N_2 was used as an internal standard in the gas chromatography (GC) determination of O_2 percentiles. The higher the TON, the more stable the catalyst. The TON of complex $[Ru^{II}(terpy)(phen)Cl]PF_6$ was used as an internal standard for consistency.[2] Because good agreement was found between our experiments and those previously reported, the TONs of complexes **1**−**4** were measured with confidence. Species **2** with an electron-withdrawing nitro group displays the lowest TON, whereas **3** and **4** with electron-donating methyl groups indicate higher activity than that of complex **2** but slightly lower than that of the unsubstituted **1**. In general terms, it has been observed[2,10] that electron-withdrawing groups in related $[Ru^{II}(terpy)(R\text{-}bipy)X]^+$ complexes (X = Cl or H_2O) lead to enhancement of the TONs. Similarly, bipy-containing electron-donating groups led to a clear decrease in the TONs. The species $[Ru^{II}(terpy)(NO_2\text{-}bipy)Cl]^+$ is an exception to this observation because its TON is slightly lower than that of the unsubstituted complex.[2] Nonetheless, the nitro complex still displays higher TONs than the equivalent species with electron-donating substituents. Considering terpy substituents on the 4′ position, an opposite trend was reported and electron-withdrawing groups led to lower TONs.[10,11] This observation points to subtle but important differences in the catalytic potential of bipy- and phen-based catalysts. On the other hand, the presence of an electron-donating Ph-SMe mercapto substituent in complex **1** has fostered a higher TON than its unsubstituted counterpart $[Ru^{II}(terpy)(phen)Cl]PF_6$, in good agreement with the literature.[11]

The amounts and rates of O_2 generated in acidic aqueous media were studied with a Clark electrode under argon for complexes **1**−**4** with an excess of $(NH_4)_2[Ce^{IV}(NO_3)_6]$ in a Ru/Ce ratio of 1:5000 equiv. For complex **1**, a first-order kinetic behavior was determined from measurements at different concentrations (Figure 3a,b), confirming that O_2 generation is dependent on the molecular procatalyst. All of the complexes required an induction period of 200−300 s prior to O_2 detection. The shortest induction period was observed for the tetramethylated **4**, while the longest was reported for the nitro species **2**. This induction period has been historically associated with conversion of the halido (Cl and Br) procatalyst[4] into the more active aqua-substituted catalyst.[10,20] Further evidence by the Thummel group suggests that the iodo procatalyst $[Ru^{II}(terpy)(bipy)I]^+$ and its aqua counterpart $[Ru^{II}(terpy)(bipy)H_2O]^+$ do not require this induction period.[4] This observation is particularly relevant for the iodo-substituted species because it presents the highest TON of 570. The rates of O_2 evolution for **1**−**4** were determined by measuring the linear portion of the curves after the induction period and before 800 s (see Table 1). The highest rate of O_2 evolution was observed for **4**, whereas complex **2** indicated the lowest rate, thus in good agreement with other published $[Ru^{II}(terpy)(bipy)Cl]^+$ species.[2]

Another important consideration in the assessment of the catalyst is the possibility of the formation of heterogeneous catalysts such as RuO_2 nanoparticles[2] or $Ce\cdots Ru^{IV}{=}O$ clusters.[21] In order to rule out the presence of heterogeneous species in solution, dynamic light scattering (DLS) was used to analyze the solutions of Ce^{IV} + triflic acid and Ce^{IV} + triflic acid + complex **1** in ACN at the same concentrations as those used for determination of the rates of O_2 generation (Figure S5 in the SI). If the induction period should involve the formation of heterogeneous species, a noticeable increase in the size distribution of the samples should become apparent. Because no heterogeneous forms were observed for any of those solutions over a period of 20 min, thus longer than the ∼5 min induction times, the notion that catalysis is based on molecular species is again reinforced. It has been accepted that the formation of a more active aqua catalyst in aqueous acidic media via substitution of the chlorido ligand for water can be inspected by UV−visible changes.[10] Furthermore, if the

dx.doi.org/10.1021/ic402118u | Inorg. Chem. 2014, 53, 3311−3319

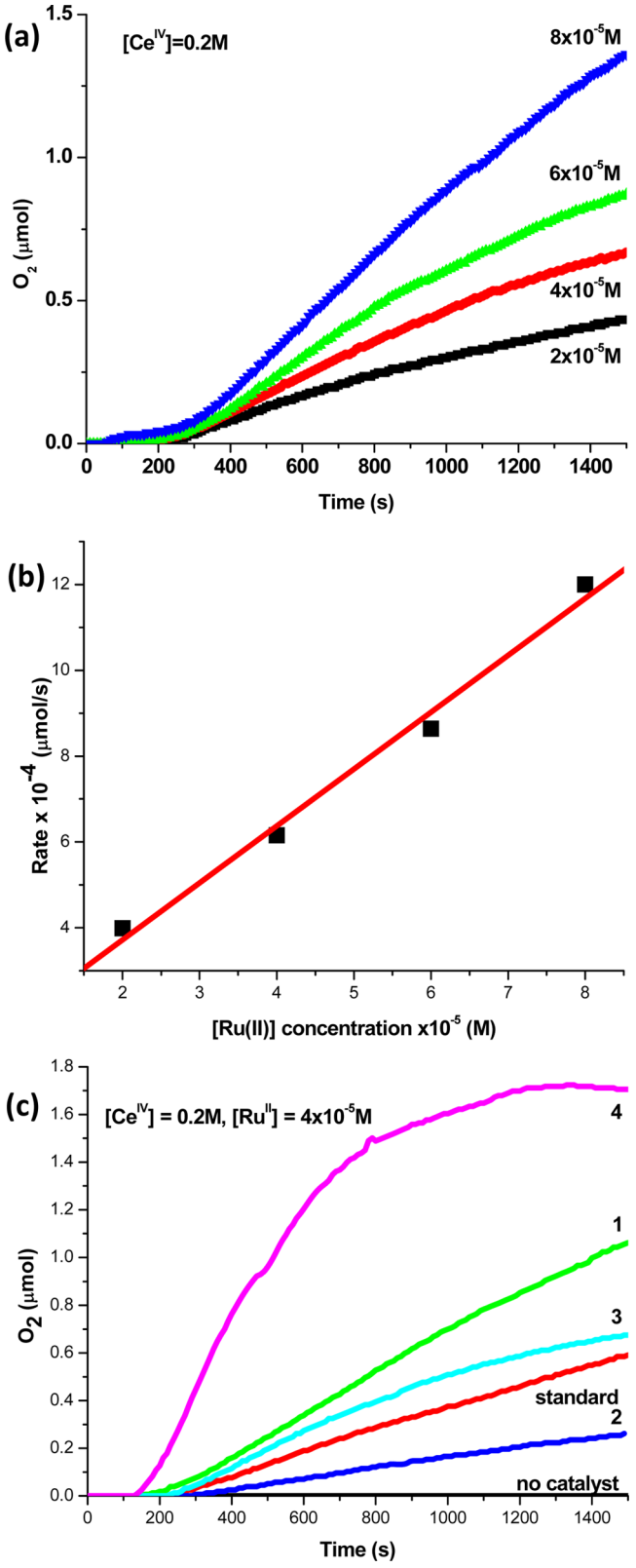

Figure 3. (a) O_2 generation with different concentrations of **1** over time. (b) First-order plot of the initial rate data for **1**. (c) Generation of O_2 as a function of time with a YSI Clark electrode for complexes **1**−**4**.

induction period observed for **1**−**4** is exclusively associated with ligand substitution in the Ru^{II} core, then the presence of Ce^{IV} is irrelevant. Therefore, UV−visible spectral changes were monitored for **1** excluding Ce^{IV} while keeping the other reaction conditions similar to those used for evaluation of the O_2 rates. Because precipitation was observed (Figure S6a in the SI), the conditions were changed to a 1:1 mixture of ACN/triflic acid (aqueous). Under these conditions and in the absence of light, conversion to the aqua complex was observed, however with a half-life of 290 min (Figure S6b in the SI). This is a 60-fold longer time than the observed 300 s, suggesting that Ce^{IV} is necessary to initiate the catalytic cycle. Further evidence of nontrivial conversion of the procatalyst **1** comes from time-dependent ^1H NMR data in ACN-d_3/D_2O following the disappearance of the peak at 13.00 ppm. This peak is associated with the phen H9 proton closest to the chlorido ligand (see Scheme 1 for the proton numbering) and is expected to shift to a more downfield value of 12.64 ppm when a water molecule replaces the chlorido ligand. We noticed that the original chlorido species remained unchanged in the first 24 h and disappeared completely after 120 h. The aqua species can be observed as a minor signal after 6 h, subsequently increasing in intensity and then existing alone after approximately 120 h (Figures 4 and S7 in the SI). A slower conversion was observed when the ACN-d_3/D_2O ratio was changed to 4:1 (Figure S8 in the SI). We also followed up the chloride-to-aqua conversion for complexes **1**−**4** in 3:1 DMSO-d_6/D_2O with triflic acid (0.1 M). In this solvent mixture, the phen H9 proton appears at 10.19 ppm, and a new peak was observed at 8.96 ppm associated with the formation of a triflate-substituted entity that is further converted into the aqua species, as observed by a peak at 9.00 ppm (Figures S9−S14 in the SI). Even in this case, the "chlorido" peak at 10.19 ppm is observed and does not disappear. Some back-conversion was observed within 3 h when LiCl was added to the aged solutions. Interestingly, the spectra of the nitro-substituted **2** do not vary over time.

Reactivity Studies. *Oxidative Titration of 1 with Ce^{IV}.* UV−visible spectroscopy has been used to monitor the reactivity of aqua-substituted catalysts toward Ce^{IV},[8] but no spectroscopic studies have been carried out with chlorido-containing procatalysts. Therefore, we have generated spectroscopic profiles for **1**−**4** associated with Ru^{III} and Ru^{IV} species by titrating against Ce^{IV} before study of the relative reactivities of these complexes. The addition of 1 equiv of Ce^{IV} to complex **1** resulted in ca. 60% decrease in the 518 nm Ru^{II} → terpy MLCT band (Figure S15 in the SI) at the same time that a new band assigned to a Ru^{III} species appeared at 413 nm. Because the 518 nm band did not disappear completely, this is indicative of either incomplete or competitive oxidation, most likely of the $-SCH_3$ substituent on the terpy ligand, as observed for aromatic thiols.[22] As shown in Figure 5a, the addition of 2 equiv of Ce^{IV} resulted in the complete disappearance of the 518 nm band and the appearance of yet another band at 360 nm, in addition to that at 413 nm. Available literature on $[Ru^{II}(terpy)(bipy)H_2O]^{2+}$ complexes assign this band to either the Ce^{IV} ion or the formation of $[Ru^{IV}{=}O]^{2+}$ species.[3,5a,b,21,8] The UV−visible spectrum of $(NH_4)_2[Ce(NO_3)_6]$ was taken in aqueous acidic media (triflic or nitric acid, pH = 1) and revealed ill-defined processes at 300 nm (abs ≤ 0.3), whereas an expected ∼350 nm Ce^{IV}-related band was not observed (Figure S16 in the SI). This reinforces the idea that the 360 nm process in **1** is associated with a high-valent ruthenium species. Titration was continued for up to 5 equiv of Ce^{IV} to monitor changes during one catalytic cycle.

Reductive Titration of 1 with Ascorbic Acid (AA). In order to verify that the observed spectroscopic profiles are associated

dx.doi.org/10.1021/ic402118u | Inorg. Chem. 2014, 53, 3311−3319

Table 1. Electronic and Water Oxidation Properties of Complexes 1−4

complex	λ_{max}, nm (ε, $M^{-1}cm^{-1}$)[a]	$E_{1/2}$ (ΔE; $\lvert I_{pa}/I_{pc}\rvert$), V)[b]	TON[c]	rate[d] × 10^{-4} (μmol of O_2 s^{-1})
1	515 (16224), 435 (sh, 7716), 318 (39614)	−1.97 (0.054; |1.4|), −1.73 (irrv), **0.40** (0.058; |1.00|), 1.05 (irrv) Fc^+/Fc = 0.44 (0.074; |1.00|)	410	8.19
2	518 (18017), 316 (40689)	−1.93 (irrv), −0.11 (irrv), **0.46** (0.072; |0.9|), 1.11 (irrv) Fc^+/Fc = 0.44 (0.075; |1.0|)	60	2.40
3	515 (15673), 429 (sh, 7492), 316 (40579)	−2.01 (0.060, |0.4|), −1.74 (irrv), **0.38** (0.063; |0.9|), 1108 (irrv) Fc^+/Fc = 0.44 (0.081; |1.0|)	250	6.92
4	520 (16997), 422 (sh, 11018), 319 (45154)	−2.14 (irrv), −1.77 (irrv), **0.33** (0.068; |0.9|), 1.07 (irrv) Fc^+/Fc = 0.44 (0.076; |1.0|)	150	27.3

[a]UV−visible spectra recorded in 5 × 10^{-5} M ACN. [b]Cyclic voltammograms of **1**−**4** recorded as 4.0 × 10^{-4} mol L^{-1} in ACN with 0.1 M $TBAPF_6$ as the supporting electrolyte using a 100 mV s^{-1} scan rate at room temperature in an inert atmosphere; WE = glassy carbon, RE = Ag/AgCl, and CE = platinum wire. All potentials listed versus Fc^+/Fc. Measured in ACN. [c]$(NH_4)_2[Ce(NO_3)_6]$ (550 mg, 1 mmol) and CF_3SO_3H (3 mL, pH = 1) were stirred together in the complex (100 μL, 8 × 10^{-5} mmol) for 24 h. [d]CF_3SO_3H (pH = 1, 5 mL), $(NH_4)_2[Ce(NO_3)_6]$ (550 mg), and the complex (4 × 10^{-5} M).

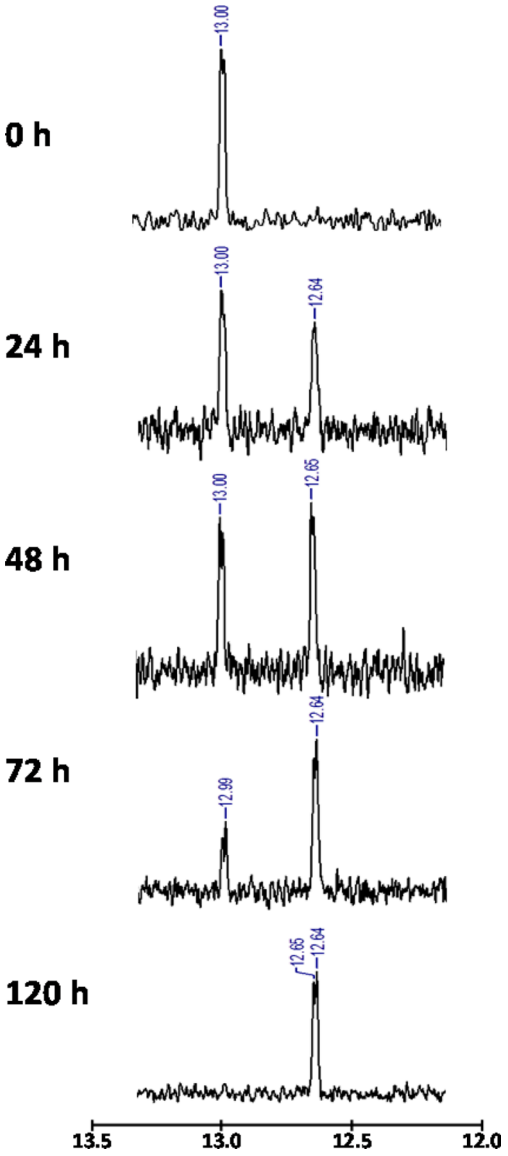

Figure 4. ^1H NMR analysis of **1** in a 1:1 ACN-d_3/D_2O mixture.

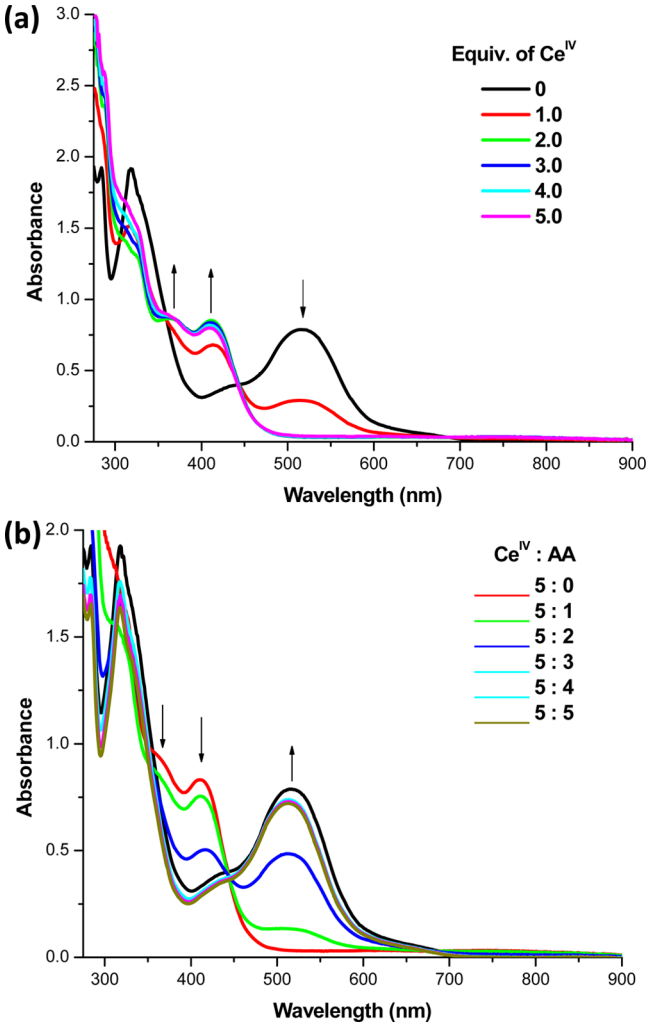

Figure 5. (a) UV−visible spectral changes for **1** (5 × 10^{-5} M in ACN, 2.5 mL) upon oxidation with Ce^{IV} (5 × 10^{-3} M in aqueous triflic acid, 25−125 μL, pH = 1). (b) UV−visible spectral changes for oxidized **1** upon reductive titration with AA in water (5 × 10^{-3} M, 25−125 μL).

with the formation of high-valent ruthenium species, likely Ru^{IV}, the same solution treated with 5 equiv of Ce^{IV} was titrated with the reducing agent AA. As illustrated in Figure 5b, the characteristic Ru^{II} → terpy MLCT band reappears at ca. 515 nm, suggesting the regeneration of Ru^{II} species. Assuming the bivalent Ru^{II} is regenerated, the next question is concerned with whether the chlorido ligand is replaced by water during the catalytic cycle. A comparison between the UV−visible data for previously published $[Ru^{II}(terpy)(phen)Cl]^+$ and $[Ru^{II}(terpy)(phen)H_2O]^{2+}$ suggests a hypsochromic shift of 22 nm for the aqua complex.[4] Because the regenerated MLCT band at 515

dx.doi.org/10.1021/ic402118u | Inorg. Chem. 2014, 53, 3311−3319

nm does not indicate significant shifts, it is possible that the chlorido group is still attached to the catalytic core. Similarly, the bands at 360 and 410 nm associated with a high-valent ruthenium species disappear, and the resulting spectrum resembles that of the starting complex **1**. In summary, **1** seems to reach higher oxidation states, while bound to the chlorido ligand. This might be possible either via the formation of a seven-coordinate $[Ru^{IV}{=}O]^{+2}$ or via the bond-breaking and flipping of one of the pyridine units in the terpy to form a six-coordinate $[Ru^{IV}{=}O]^{+}$ species. Although further mechanistic evaluation will be required, complexes **1**−**4** would most likely follow the latter case. The former mechanism has been verified in $[Ru^{II}(pda)L_2]$ (pda = 1,10 phenanthrolinedicarboxylic acid; L = pyridine), where a large O−Ru−O angle grants access of water to the ruthenium core.[23]

Time-dependent Decomposition of High-valent Ruthenium Species. Changes in the electronic absorption spectra of complex **1** upon reaction with 5 equiv of Ce^{IV} are shown in Figure 6a. The MLCT band at 518 nm disappeared

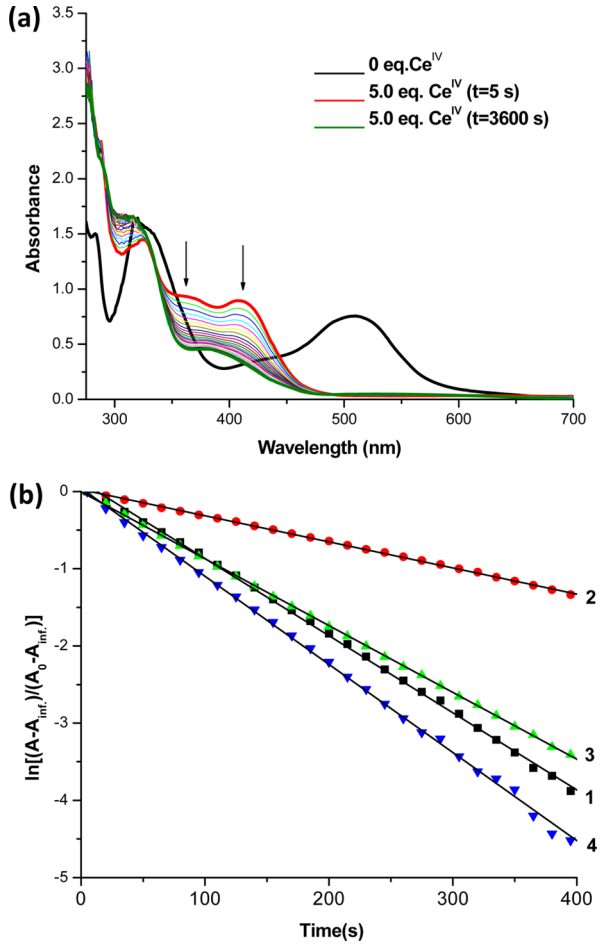

Figure 6. (a) Spectral changes for **1** over time with a Ru^{II}/Ce^{IV} ratio of 1:5, $[Ru^{II}] = 1 \times 10^{-4}$ M, 1.5 mL in ACN, $[Ce^{IV}] = 5 \times 10^{-4}$ M, 1.5 mL in triflic acid (pH = 1). (b) First-order rate profiles for **1**−**4**.

immediately after the addition of 5 equiv of an excess of the oxidant. A similar observation has been reported,[21] where a comparable band on $[Ru^{II}(terpy)(bipy)H_2O]^{2+}$ disappeared within 1.2 s upon the addition of a 10-fold excess of Ce^{IV}. Over time, the new bands at 360 and 410 nm for **1** decreased, while a 325 nm band increased. The relative rate of decay of the 360 nm band in **1**−**4** was calculated along with the first-order decay plots in Figure 6b. Complex **4** shows the highest rate of decay (11.4×10^{-3} s^{-1}), followed by species **1** and **3** (9.9×10^{-3} and 8.6×10^{-3} s^{-1}, respectively). The rate observed for **2** reaches 3.4×10^{-3} s^{-1} and is much slower than that of **4**. This trend is in good agreement with the observed rates of O_2 evolution discussed previously, and the half-lives for the decay of **1**−**4** are comparable to the induction period observed for the rate of O_2 evolution (Table T1 in the SI).

Evaluation of the Recovered Procatalyst. The results outlined in the previous sections suggest that the catalytic core in these species is regenerated after catalysis. We have recovered and isolated the catalyst in order to address this question in further detail. Complex **1** was treated with a 60-fold excess of Ce^{IV} in aqueous triflic acid, yielding an air-unstable green precipitate after 24 h. This precipitate was isolated by filtration, dissolved in DMSO, and analyzed by ^1H NMR spectroscopy and ESI-MS in the positive mode. Broad peaks observed in the ^1H NMR spectrum of the precipitate are suggestive of a paramagnetic high oxidation state different from that of the low-spin $4d^6$ Ru^{II} present in **1**. In order to verify whether the catalytic core is preserved during catalysis, AA was added to this species, prompting an immediate color change from green to red. The ^1H NMR spectrum of the resulting red species was recorded in DMSO and compared with **1** before catalysis. Proton labeling for **1** is shown in Scheme 1 and Figure 7, and the phen H9 proton at 10.32 ppm remained unchanged in the recovered catalyst. This fact is interpreted as having the chlorido group still coordinated to the ruthenium center. However, peak shifts at 9.20, 8.33, and 7.58 ppm suggest structural alteration associated with the terpy of the recovered catalyst. Because the proton counts of the aromatic region in both spectra are equivalent, the structural change must be associated with oxidation of the −SMe group into a $-SO_2Me$ group. This oxidation has been confirmed by ESI-MS analysis (Figure S17 in the SI), where a molecular ion peak at m/z 703.91 is observed. This peak is 32 mass units higher than that of the parent peak $[Ru^{II}(MeMPTP)(phen)Cl]^+$ for **1**. As added evidence for this conversion, the equivalent species $[Ru^{II}(terpy)(phen)Cl]^+$ failed to show such mass modification and retained its original mass (Figure S18 in the SI). Furthermore, the ligand MeMPTP was treated with Ce^{IV}, yielding the oxidized product, as observed by IR spectroscopy with an S=O band at 1298 cm^{-1} and ESI-MS where peaks at m/z 372.1337 and 388.1302 are observed for the $-SOCH_3$ and $-SO_2CH_3$ species (Figures S19 and S20 in the SI). The mother liquor recovered after precipitation of the green species was also isolated and analyzed by ESI-MS in the positive and negative modes. No measurable quantities of any ruthenium species was detected either as discrete catalysts or in Ru/Ce clusters.[21]

CONCLUSIONS

The water oxidation ability of ruthenium/MeMPTP complexes with several substituted phen ligands was analyzed by evaluation of their TONs and rates of O_2 generation. Although we treated these species as "procatalysts" to follow the established nomenclature that considers the aqua-substituted counterparts as "catalysts", the observed TONs for both classes of compounds are comparable. We can summarize our observations as follows: (i) The catalytic O_2 generation requires the presence of Ce^{IV}. (ii) The catalytic activity was enhanced by the presence of electron-donating groups on the phen, while the presence of electron-withdrawing substituents

dx.doi.org/10.1021/ic402118u | Inorg. Chem. 2014, 53, 3311−3319

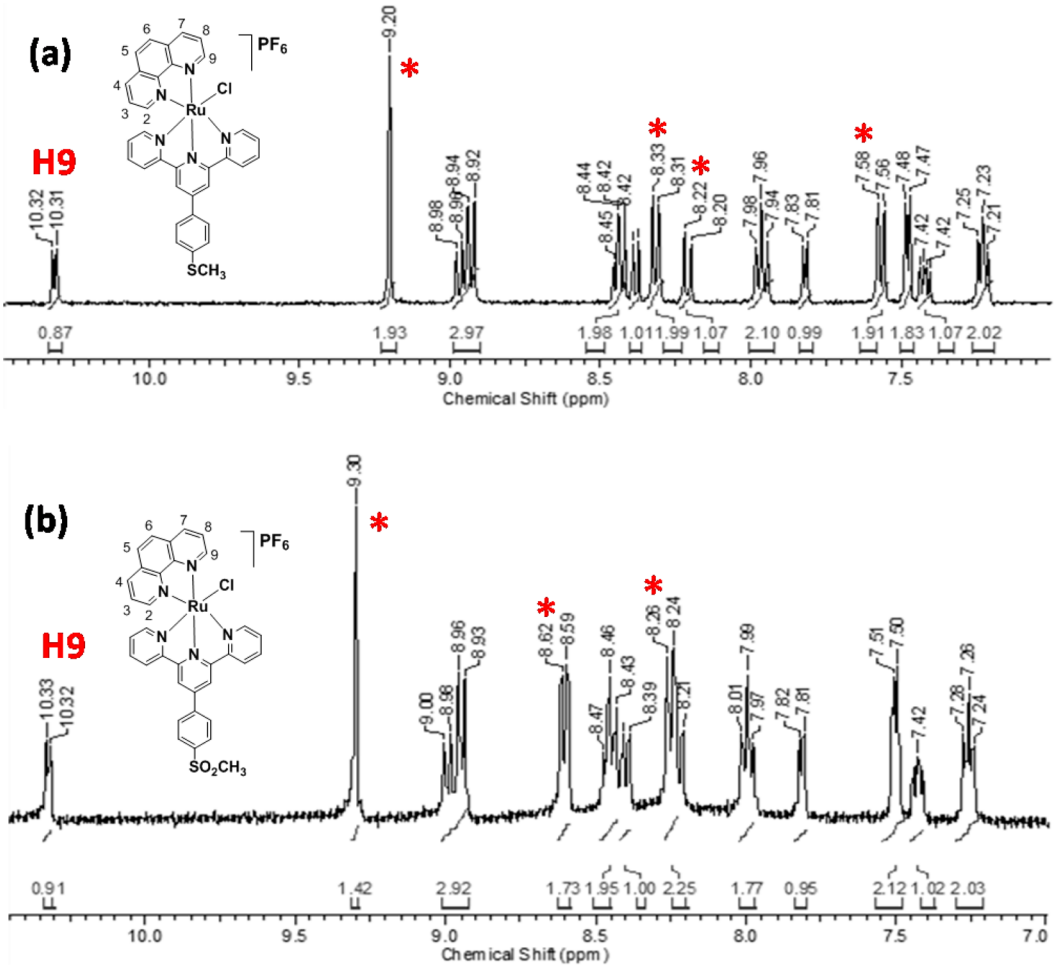

Figure 7. ^{1}H NMR spectra in DMSO for **1** (a) before and (b) after catalysis.

decreases it drastically. This effect is explained by the fact that the $-NO_2$ group in **2** decreases the electronic density on the phen ligand, making it difficult to achieve higher oxidation states relevant for catalysis, whereas the weakly donating $-CH_3$ groups in **3** and **4** activate the phen ligand, facilitating the generation of those high-valent ruthenium states. As such, TONs follow the sequence **1** > **3** > **4** > **2**, while the rates of O_2 evolution follow **4** > **1** > **3** > **2**. (iii) All species require an induction period for catalysis, and the rates of O_2 generation follow a first-order mechanism in the presence of excess Ce^{IV}. (iv) Spectroscopic evidence suggests that, during the induction period, high oxidation species (possibly Ru^{IV} at 360 nm) are generated, but no evidence of chloride-by-water exchange was observed. Heterogeneous forms of the catalyst were ruled out by DLS. (v) A decrease of the 360 nm band, related to $Ru^V{=}O$ generation, associates the highest rates of decay in the order **4** > **1** > **3** > **2**; this may be an indication that the position, as well as the nature of the substituent, plays a role in catalysis. (vi) Rather than an obvious chloride-by-water exchange, the catalytic core seems to remain unchanged even in the presence of excess Ce^{IV}, thus favoring either a seven-coordinate intermediate or a six-coordinate route where a pyridine group on MeMPTP gets uncoordinated. (iv) The presence of the electron-donating $-$PhSMe group on MeMPTP enhances the catalytic activity, although it undergoes oxidation to $-SO_2Me$ in the presence of Ce^{IV}. These results highlight significant differences between phen- and bipy-based procatalysts, point to unique electronic nuances of the phen unit, and will be pivotal for the design and optimization of future water oxidation catalysts. Future studies will focus on the mechanistic details of the catalytic cycle for **1**–**4**, the evaluation of the catalytic activity in multimetallic topologies based on phen functionalization, and the use of MeMPTP for self-assembly on gold electrodes.

■ EXPERIMENTAL SECTION

Materials and Methods. Reagents and solvents were used as received from commercial sources. Methanol and ethanol were distilled over CaH_2. 1,10-Phenanthroline, 1-(pyridin-2-yl)ethanone, and 4-(methylthio)benzaldehyde were purchased from Alfa Aesar, $RuCl_3$ was purchased from Strem Chemicals, and 5,6-dimethylphenanthroline was purchased from GFS Chemicals Inc. 5-Nitrophenanthroline was synthesized according to known procedures.[24] IR spectra were measured from 4000 to 400 cm^{-1} as KBr pellets on a Tensor 27 FTIR spectrophotometer. ^{1}H NMR spectra were measured using Varian 400 mHz spectrometers. ESI-MS spectra (positive) were measured in either a triple-quadrupole Micromass QuattroLC or a single-quadrupole Waters ZQ2000 mass spectrometer with an electrospray/APCI or ESCi source. Experimental assignments were simulated on the basis of the peak position and isotopic distributions. Elemental analyses were performed by Midwest Microlab, Indianapolis, IN. UV–visible spectroscopy from 5.0×10^{-5} M ACN solutions was performed using a Cary 50 spectrophotometer in the range of 250–1100 nm. Cyclic voltammetry experiments were performed using a BAS 50W voltammetric analyzer. A standard three-electrode cell was employed with a glassy-carbon working electrode, a platinum wire auxiliary

dx.doi.org/10.1021/ic402118u | Inorg. Chem. 2014, 53, 3311–3319

electrode, and an Ag/AgCl reference electrode under an inert atmosphere at room temperature. The salt $TBAPF_6$ (TBA = tetrabutylammonium) was used as the supporting electrolyte. Potentials are presented using ferrocene[25] as the internal standard. DLS experiments were performed in a Zetasizer Nano Series spectrophotometer using $[Ce^{IV}]$ = 0.2 M in triflic acid, 2.5 mL, pH = 1, and complex **1** at 5×10^{-5} M (1.98 mg/0.5 mL, injecting 25 μL).

Water Oxidation. Studies were carried out in a 10 mL round-bottomed flask capped with a rubber septum under ambient conditions. $(NH_4)_2[Ce(NO_3)_6]$ (550 mg, 1 mmol) and CF_3SO_3H (3 mL, pH = 1) were stirred together, the complex (100 μL, 8×10^{-5} mmol) dissolved in ACN was injected through the septum, and the mixture was allowed to react for 24 h. The amount of O_2 generated was measured with a gas chromatograph by injecting 100 μL of a headspace gas sample. The gas chromatograph is a Gow-Mac 400 with a thermal conductivity detector, and a 8 ft × $^1/_8$ in., 5 Å molecular sieve column operating at 60 °C was used with helium as the carrier gas. The calibration was carried out with air as the standard (21% O_2). The TON was calculated as the ratio of moles of O_2 produced over moles of catalyst used. *Clarity* software was used for data acquisition from GC. The rate of O_2 evolution was carried out in a three-necked flask charged with triflic acid (pH = 1, 5 mL) and $(NH_4)_2[Ce(NO_3)_6]$ (550 mg) under an argon atmosphere, following well-established protocols available in the literature.[4] Prior to injection of the complex, the YSI Clark-type electrode was calibrated with O_2, argon, and air-saturated solutions. After calibration, water saturated with air indicated the O_2 percentage in solution as 20 ± 1%. Then the complex (50 μL, 4×10^{-5} M, AcN) was injected, and O_2 percentage reading was recorded every 10 s up to 40 min.

X-ray Structural Determinations. Diffraction data were measured on a Bruker X8 APEX-II Kappa geometry diffractometer with Mo radiation and a graphite monochromator. Frames were collected at 100 K with the detector at 40 mm and 0.3° between each frame and were recorded for 10 s. *APEX-IIa* and *SHELXb* software were used in the collection and refinement of the models. Crystals of **3** appeared as dark plates. A total of 23546 reflections were measured, yielding 9818 unique data (R_{int} = 0.104). Hydrogen atoms were placed in calculated positions. These cationic complexes **1** crystallized with 1 equiv of PF_6^- and 3 equiv of ACN. The anion showed typical PF_6^- disorder in the F positions, as evidenced by the high thermal parameters for these atoms. Crystals of **4** were dark fragments. A total of 72908 reflections were counted, which averaged to 10161 independent data (R_{int} = 0.054). H atoms were placed at calculated positions. The cationic complex crystallized with one PF_6^- anion and 2 equiv of ACN. Disorder in the PF_6^- anion was handled by assigning partial occupancy positions for four of the F atoms. These partial contributions were held isotropic.[26] Table 2 summarized the data for both structures.

Syntheses. *Ligand 4′-(4-Methylmercaptophenyl)-2,2′:6′2″-terpyridine (MeMPTP).* The ligand MeMPTP was prepared according to literature procedures[17] by treating 2 equiv of 2-acetylpyridine with 1 equiv of 4-(methylthio)benzaldehyde. Figure S21 in the SI summarizes the NMR data.

$[Ru^{II}(MeMPTP)(DMSO)Cl_2]$. A mixture of $[Ru^{II}(DMSO)_4Cl_2]$[26] (0.696 g, 1.44 mmol) and MeMPTP (0.512 g, 1.44 mmol) was heated and refluxed in argon-degassed CH_3OH (50 mL) for 7 h. The solution turned brownish red, and a dark-brown precipitate was formed. The precipitate was isolated by frit filtration and washed with cold CH_3OH (3 × 10 mL). Yield: 510 g (58%). ^1H NMR (DMSO-d_6): δ 9.01 (d, J = 4.9 Hz, 2H), 8.84 (s, 2H), 8.77 (d, J = 8.1 Hz, 2H), 8.14 (m, 4H), 7.78 (m, 2H), 7.46 (d, J = 8.1 Hz, 2H), 3.59 (s, 3H). MS: m/z 601.95 ($[C_{24}H_{23}Cl_2N_3ORuS_2]^+$). FTIR (KBr, cm^{-1}): 1054.26 (S=O stretch of DMSO), 2956.22 (C−H stretch of the *tert*-butyl substituent). UV−visible [DMSO; λ_{max}, nm (ε, M^{-1} cm^{-1})]: 291 (29681), 338 (36703), 400 (9323), 530 (11255), 680 (5471).

*$[Ru^{II}(MeMPTP)(phen)Cl]PF_6$ (**1**).* A mixture of $[Ru^{II}$(MeMPTP)-(DMSO)$Cl_2]$ (0.241 g, 0.4 mmol), 1,10-phenanthroline (0.072g, 0.4 mmol), and triethylamine (0.5 mL) in CH_3OH (50 mL) was refluxed in the dark overnight under argon. The volume of the resulting solution was reduced to one-third, and NH_4PF_6 (0.50 g) was added. The dark-red precipitate was isolated over a frit and washed with CH_3OH (3 × 10 mL). The purified **1** was obtained after column chromatography over neutral alumina with CH_2Cl_2/CH_3CN (1:1). Yield: 183 mg (56%). Elem anal. Calcd for $C_{34}H_{25}ClN_5RuSPF_6$: C, 49.97; H, 3.18; N, 8.57. Found: C, 49.91; H, 3.23; N, 8.47. ^1H NMR (DMSO-d_6): δ 10.32 (br s, 1H), 9.2 (m, 2H), 8.95 (m, 4H), 8.42 (d, J = 5.7 Hz, 2H), 8.38 (d, J = 7.3 Hz, 1H), 8.31 (d, J = 8.1 Hz, 2H), 8.21 (m, 1H), 7.95 (m, 2H), 7.82 (d, J = 5.7 Hz, 1H), 7.56 (d, J = 8.1 Hz, 2H), 7.48 (d, J = 4.1 Hz, 2H), 7.42 (br s, 1H), 7.23 (d, J = 5.7 Hz, 2H), 2.63 (s, 3H). MS: m/z 672.06 ($[C_{34}H_{25}ClN_5RuS]^+$). FTIR (KBr, cm^{-1}): 1596.58, 1476.03, 1426.85, 1406.31 (pyridine rings), 841.43 (PF_6^-).

Complexes **2**−**4** were synthesized in a manner similar to that described for **1**. Analyses follow.

*$[Ru^{II}(MeMPTP)(NO_2$-phen$)Cl]PF_6$ (**2**).* Yield: 109 mg (42%). Elem anal. Calcd for $C_{34}H_{24}ClN_6O_2RuSPF_6$: C, 47.37; H, 2.81; N, 9.75. Found: C, 47.38; H, 2.82; N, 9.51. ^1H NMR (DMSO-d_6): δ 10.46 (m, 1H), 9.28 (m, 2H), 9.2 (m, 3H), 8.94 (d, J = 7.3 Hz, 2H), 8.57 (m, 2H), 8.32 (d, J = 8.1 Hz, 2H), 8.07 (d, J = 4.1 Hz, 1H), 8.00 (m, 2H), 7.54 (m, 4H), 7.23 (m, 2H), 2.62 (s, 3H). MS: m/z 717.0417 ($[C_{34}H_{24}ClN_6O_2RuS]^+$). FTIR (KBr, cm^{-1}): 1595.12, 1532.80, 1425.13, 1406.12, 1406.31 (pyridine rings), 1329.31 ($-NO_2$), 843.28 (PF_6^-).

*$[Ru^{II}(MeMPTP)(Me_2$-phen$)Cl]PF_6$ (**3**).* Yield: 55 mg (32%). Elem anal. Calcd for $C_{36}H_{29}ClN_5RuSPF_6$: C, 51.16; H, 3.46; N, 8.29. Found: C, 50.96; H, 3.64; N, 8.27. ^1H NMR (DMSO-d_6): δ 10.31 (d, J = 4.86 Hz, 1H), 9.20 (s, 2H), 9.08 (d, J = 8.11 Hz, 1H), 8.93 (d, J = 8.11 Hz, 2H), 8.45 (m, 2H), 8.31 (d, J = 8.92 Hz, 2H), 7.96 (t, J = 7.70 Hz, 2H), 7.74 (d, J = 5.67 Hz, 1H), 7.56 (d, J = 8.11 Hz, 2H), 7.43 (d, J = 5.67 Hz, 2H), 7.40 (m, 1H), 7.22 (m, 2H), 2.9 (s, 3H), 2.71 (s, 3H), 2.62 (s, 3H). MS: m/z 700.0878 ($[C_{36}H_{29}ClN_5RuS]^+$). FTIR (KBr, cm^{-1}): 2921.46 (C−H stretch in the $-CH_3$ group), 1595.13, 1501.43, 1476.47 (pyridine rings), 844.16 (PF_6^-).

*$[Ru^{II}(MeMPTP)(Me_4$-phen$)Cl]PF_6$ (**4**).* Yield: 95 mg (34%). Elem anal. Calcd for $C_{38}H_{33}ClN_5RuSPF_6$: C, 52.27; H, 3.81; N, 8.02. Found: C, 52.33; H, 4.03; N, 7.96. ^1H NMR (DMSO-d_6): δ 10.05 (m, 1H), 9.17 (m, 2H), 8.91 (d, J = 8.1 Hz, 2H), 8.54 (m, 1H), 8.32 (m, 3H), 7.94 (m, 2H), 7.56 (m, 2H), 7.47 (m, 3H), 7.22 (m, 2H), 3.00 (s, 3H), 2.79 (s, 3H), 2.62 (s, 3H), 2.56 (s, 3H), 2.08 (s, 3H). MS: m/z 728.1174 ($[C_{38}H_{33}ClN_5RuS]^+$). FTIR (KBr, cm^{-1}): 2924.46 (C−H stretch in the $-CH_3$ group), 1592.64, 1466.68, 1425.27 (pyridine rings), 842.68 (PF_6^-).

Table 2. X-ray Data

	[3]·$^1/_3CH_3CN$	[4]·$^1/_2CH_3CN$
formula	$C_{42}H_{38}ClF_6N_8PRuS$	$C_{42}H_{39}ClF_6N_7PRuS$
fw	968.35	955.35
space group	triclinic, $P\bar{1}$	monoclinic, $P21/c$
a (Å)	8.8581(7)	15.7842(8)
b (Å)	15.4618(11)	13.1866(7)
c (Å)	16.0397(12)	19.5857(10)
α (deg)	103.240(4)	90
β (deg)	105.443(4)	93.825(2)
γ (deg)	91.864(4)	90
V (Å^3)	2051.0(3)	4067.5(4)
Z	2	4
T (K)	100(2)	100(2)
λ (Å)	0.71073	0.71073
ρ (mg m^{-3})	1.568	1.560
μ (mm^{-1})	0.608	0.611
$R(F)$ (%)	12.27	0.0419
$R_w(F)$ (%)	18.55	0.0504

[a] $R(F) = \sum||F_o| - |F_c||/\sum|F_o|$; $R_w(F) = [\sum w(F_o^2 - F_c^{2)2}/\sum w(F_o^2)^2]^{1/2}$ for $I > 2\sigma(I)$.

dx.doi.org/10.1021/ic402118u | *Inorg. Chem.* 2014, 53, 3311−3319

■ ASSOCIATED CONTENT

Supporting Information

X-ray crystallographic data in CIF format, table of rate data, structure of complex **1**, cyclic voltammograms, UV−visible and FTIR spectra, DLS, precipitation of complex **1**, ^{1}H NMR and MS analysis, and ESI (positive) isotope distribution. This material is available free of charge via the Internet at http://pubs.acs.org.

■ AUTHOR INFORMATION

Corresponding Author

*E-mail: cnverani@chem.wayne.edu. Phone: 313 577 1076.

Notes

The authors declare no competing financial interest.

■ ACKNOWLEDGMENTS

This research was made possible by the Division of Chemical Sciences, Geosciences, and Biosciences, Office of Basic Energy Sciences, of the U.S. Department of Energy through the Single-Investigator and Small-Group Research (Solar Energy Program Grants DE-SC0001907 and DE-FG02-09ER16120 to C.N.V.), including financial support for D.C.W. We thank Prof. John Endicott at WSU for insightful discussions and suggestions, Gayani Dedduwa Mudalige and Prof. Christine Chow for measurement of the DLS profiles for complex **1**, and Chenchen He and Prof. M. T. Rodgers for the exact ESI-MS of the oxidized ligand MeMPTP^{SO_2CH_3}.

■ REFERENCES

(1) (a) Brimblecombe, R.; Dismukes, G. C.; Swiegers, G. F.; Spiccia, L. *Dalton Trans.* **2009**, *43*, 9374−9384. (b) Wasylenko, D. J.; Palmer, R. D.; Berlinguette, C. P. *Chem. Commun.* **2013**, *49*, 218−227. (c) Concepcion, J. J.; Jurss, J. W.; Brennaman, M. K.; Hoertz, P. G.; Patrocinio, A. O. T.; Murakami Iha, N. Y.; Templeton, J. L.; Meyer, T. J. *Acc. Chem. Res.* **2009**, *42*, 1954−1965. (d) Lewis, N. S.; Nocera, D. G. *Proc. Natl. Acad. Sci. U. S. A.* **2006**, *103*, 15729−15735.

(2) Tseng, H.-W.; Zong, R.; Muckerman, J. T.; Thummel, R. *Inorg. Chem.* **2008**, *47*, 11763−11773.

(3) Concepcion, J. J.; Jurss, J. W.; Templeton, J. L.; Meyer, T. J. *J. Am. Chem. Soc.* **2008**, *130*, 16462−16463.

(4) Kaveevivitchai, N.; Zong, R.; Tseng, H.-W.; Chitta, R.; Thummel, R. P. *Inorg. Chem.* **2012**, *51*, 2930−2939.

(5) (a) Lin, X.; Hu, X.; Concepcion, J. J.; Chen, Z.; Liu, S.; Meyer, T. J.; Yang, W. *Proc. Natl. Acad. Sci. U. S. A.* **2012**, *109*, 15669−15672. (b) Concepcion, J. J.; Tsai, M.-K.; Muckerman, J. T.; Meyer, T. J. *J. Am. Chem. Soc.* **2010**, *132*, 1545−1557. (c) Chen, Z.; Concepcion, J. J.; Luo, H.; Hull, J. F.; Paul, A.; Meyer, T. J. *J. Am. Chem. Soc.* **2010**, *132*, 17670−17673.

(6) Gilbert, J. A.; Eggleston, D. S.; Murphy, W. R.; Geselowitz, D. A.; Gersten, S. W.; Hodgson, D. J.; Meyer, T. J. *J. Am. Chem. Soc.* **1985**, *107*, 3855−3864.

(7) Jurss, J. W.; Concepcion, J. C.; Norris, M. R.; Templeton, J. L.; Meyer, T. J. *Inorg. Chem.* **2010**, *49*, 3980−3982.

(8) Wasylenko, D. J.; Ganesamoorthy, C.; Henderson, M. A.; Koivisto, B. D.; Osthoff, H. D.; Berlinguette, C. P. *J. Am. Chem. Soc.* **2010**, *132*, 16094−16106.

(9) Roeser, S.; Farràs, P.; Bozoglian, F.; Martínez-Belmonte, M.; Benet-Buchholz, J.; Llobet, A. *ChemSusChem* **2011**, *4*, 197−207.

(10) Wasylenko, D. J.; Ganesamoorthy, C.; Koivisto, B. D.; Henderson, M. A.; Berlinguette, C. P. *Inorg. Chem.* **2010**, *49*, 2202−2209.

(11) Yagi, M.; Tajima, S.; Komi, M.; Yamazaki, H. *Dalton Trans.* **2011**, *40*, 3802−3804.

(12) Lesh, F. D.; Allard, M. M.; Shanmugam, R.; Hryhorczuk, L. M.; Endicott, J. F.; Schlegel, H. B.; Verani, C. N. *Inorg. Chem.* **2011**, *50*, 969−977.

(13) Lesh, F. D.; Shanmugam, R.; Allard, M. M.; Lanznaster, M.; Heeg, M. J.; Rodgers, M. T.; Shearer, J. M.; Verani, C. N. *Inorg. Chem.* **2010**, *49*, 7226−7228.

(14) Lanznaster, M.; Heeg, M. J.; Yee, G. T.; McGarvey, B. R.; Verani, C. N. *Inorg. Chem.* **2006**, *46*, 72−78.

(15) Mulfort, K. L.; Mukherjee, A.; Kokhan, O.; Du, P.; Tiede, D. M. *Chem. Soc. Rev.* **2013**, *42*, 2215−2227.

(16) Knoll, J. D.; Arachchige, S. M.; Brewer, K. J. *ChemSusChem* **2011**, *4*, 252−261.

(17) (a) Smith, C. B.; Raston, C. L.; Sobolev, A. N. *Green Chem.* **2005**, *7*, 650−654. (b) Tuccitto, N.; Torrisi, V.; Cavazzini, M.; Morotti, T.; Puntoriero, F.; Quici, S.; Campagna, S.; Licciardello, A. *ChemPhysChem* **2007**, *8*, 227−230. (c) Wang, J.; Hanan, G. S. *Synlett* **2005**, 1251−1254.

(18) Bonnet, S.; Collin, J.-P.; Gruber, N.; Sauvage, J.-P.; Schofield, E. R. *Dalton Trans.* **2003**, 4654−4662.

(19) Tsai, C.-N.; Allard, M. M.; Lord, R. L.; Luo, D.-W.; Chen, Y.-J.; Schlegel, H. B.; Endicott, J. F. *Inorg. Chem.* **2011**, *50*, 11965−11977.

(20) Masaoka, S.; Sakai, K. *Chem. Lett.* **2009**, *38*, 182−183.

(21) Kimoto, A.; Yamauchi, K.; Yoshida, M.; Masaoka, S.; Sakai, K. *Chem. Commun.* **2012**, *48*, 239−241.

(22) (a) Farràs, P.; Maji, S.; Benet-Buchholz, J.; Llobet, A. *Chem.—Eur. J.* **2013**, *19*, 7162−7172. (b) Guillo, P.; Hamelin, O.; Batat, P.; Jonusauskas, G.; McClenaghan, N. D.; Ménage, S. *Inorg. Chem.* **2012**, *51*, 2222−2230.

(23) Tong, L.; Duan, L.; Xu, Y.; Privalov, T.; Sun, L. *Angew. Chem., Int. Ed.* **2011**, *50*, 445−449.

(24) (a) Bolger, J.; Gourdon, A.; Ishow, E.; Launay, J.-P. *Inorg. Chem.* **1996**, *35*, 2937−2944. (b) Liu, T.; Hu, J.; Yin, J.; Zhang, Y.; Li, C.; Liu, S. *Chem. Mater.* **2009**, *21*, 3439−3446.

(25) Gagne, R. K. C.; Licenski, G. *Inorg. Chem.* **1980**, *19*, 2854.

(26) Dulière, E.; Devillers, M.; Marchand-Brynaert, J. *Organometallics* **2003**, *22*, 804−811.